Phys. Lett. B 880 (2026) 140742

Contents lists available at ScienceDirect

Physics Letters B

journal homepage: www.elsevier.com/locate/physletb

Letter

Quasielastic $\overrightarrow{^3\mathrm{He}}(\vec{e}, e')$ asymmetry in the threshold region with a longitudinally polarized target

M. Nycz [a,*], W. Armstrong [b], T. Averett [c], C. Ayerbe Gayoso [c], X. Bai [a], J. Bane [d], S. Barcus [e], J. Benesch [e], H. Bhatt [f], D. Bhetuwal [f], D. Biswas [g], A. Camsonne [e], G.D. Cates [a], J-P. Chen [e], J. Chen [c], M. Chen [a], C. Cotton [a], M.M. Dalton [e], A. Deltuva [h], A. Deur [e], B. Dhital [i], B. Duran [j], S.C. Dusa [e], I. Fernando [g], E. Fuchey [k], B.R. Gamage [e], H. Gao [l], D. Gaskell [e], T. Gautam [g], N. Gauthier [e], J. Golak [m], J.-O. Hansen [e], F. Hauenstein [i], W. Henry [e], D.W. Higinbotham [e], G.M. Huber [n], C. Jantzi [a], S. Jia [j], K. Jin [a], M. Jones [e], S. Joosten [b], A. Karki [f], B. Karki [o], S. Katugampola [a], S. Kay [n], C. Keppel [e], E. King [p], P. King [o], W. Korsch [q], V. Kumar [n], R. Li [j], S. Li [r], W. Li [c], D. Mack [e], S. Malace [e], P. Markowitz [s], J. Matter [a], M. McCaughan [e], Z-E. Meziani [j], R. Michaels [e], A. Mkrtchyan [t], H. Mkrtchyan [t], C. Morean [d], V. Nelyubin [a], H. Nguyen [a], G. Niculescu [u], M. Niculescu [u], C. Peng [b], S. Premathilake [a], A. Puckett [k], A. Rathnayake [a], M. Rehfuss [j], P. Reimer [b], G. Riley [r], Y. Roblin [e], J. Roche [o], M. Roy [q], P.U. Sauer [v], S. Scopeta [w], M. Satnik [c], B. Sawatzky [e], S. Seeds [k], S. Širca [x,y], R. Skibiński [m], G. Smith [e], N. Sparveris [j], H. Szumila-Vance [e], A. Tadepalli [e], V. Tadevosyan [t], Y. Tian [p], W.A. Tobias [a], A. Usman [n], H. Voskanyan [t], H. Witała [m], S. Wood [e], B. Yale [c], C. Yero [s], A. Yoon [z], J. Zhang [a], Z. Zhao [l], X. Zheng [a], J. Zhou [l]

[a] University of Virginia, Charlottesville, Virginia, 22904, USA
[b] Argonne National Laboratory, Lemont, Illinois, 60439, USA
[c] William & Mary, Williamsburg, Virginia, 23187, USA
[d] University of Tennessee Knoxville, Tennessee, 37996, USA
[e] Thomas Jefferson National Accelerator Facility, Newport News, Virginia, 23606, USA
[f] Mississippi State University, Mississippi State, Mississippi, 39762, USA
[g] Hampton University Hampton, Virginia, 23669, USA
[h] Institute of Theoretical Physics and Astronomy, Vilnius University, Saulėtekio al. 3, LT-10257, Vilnius, Lithuania
[i] Old Dominion University Norfolk, Virginia, 23529, USA
[j] Temple University Philadelphia, Pennsylvania, 19122, USA
[k] University of Connecticut Storrs, Connecticut, 06269, USA
[l] Duke University Durham, North Carolina, 27708, USA
[m] Faculty of Physics, Astronomy and Applied Computer Science, Jagiellonian University, PL-30348, Kraków, Poland
[n] University of Regina Regina, Saskatchewan, S4S 0A2, Canada
[o] Ohio University Athens, Ohio, 45701, USA
[p] Syracuse University Syracuse, New York, 13244, USA
[q] University of Kentucky Lexington, Kentucky, 40506, USA
[r] University of New Hampshire Durham, New Hampshire, 03824, USA
[s] Florida International University Miami, Florida, 33199, USA
[t] AANL, 2 Alikhanian Brothers Street, 0036, Yerevan, Armenia
[u] James Madison University Harrisonburg, VA 22801, USA
[v] Institut für Theoretische Physik, Universität Hannover, Hannover, D-30167, Germany
[w] Dipartimento di Fisica e Geologia, Università degli Studi di Perugia and Istituto Nazionale di Fisica Nucleare, Sezione di Perugia via A. Pascoli, I - 06123 Perugia, Italy
[x] Faculty of Mathematics and Physics, University of Ljubljana, Ljubljana, 1000, Slovenia
[y] Jožef Stefan Institute, Ljubljana, 1000, Slovenia
[z] Christopher Newport University, Newport News, Virginia, 23606, USA

* Corresponding author.
E-mail address: mnycz@jlab.org (M. Nycz).

https://doi.org/10.1016/j.physletb.2026.140742
Received 8 December 2025; Received in revised form 28 May 2026; Accepted 8 July 2026
Available online 10 July 2026
0370-2693/© 2026 The Author(s). Published by Elsevier B.V. Funded by SCOAP³. This is an open access article under the CC BY license (http://creativecommons.org/licenses/by/4.0/).

ARTICLE INFO

Editor: Silvia Monica Lenzi

Keywords:
Few-body nuclei
Quasielastic scattering
Polarized ^{3}He
Final-state interactions
Meson-exchange currents

ABSTRACT

We report on the measurements of the double-spin asymmetry from electron-^{3}He scattering in the threshold region of two- and three-body breakup of ^{3}He for 4-momentum transfer values of 0.1 and 0.2 (GeV/c)^2. The measurement was done at Jefferson Lab using a polarized ^{3}He target with its spin aligned parallel to the beam direction. This asymmetry is sensitive to a combination of spin-dependent response functions not previously measured and may highlight differences in two body forces, meson-exchange currents and final-state interactions. The results of this measurement serve as a test of our understanding of few-body systems. When compared with calculations from plane wave impulse approximation and Faddeev calculations, we found that the latter, which use modern nuclear potentials and prescriptions for meson-exchange currents, demonstrate an overall good agreement with data.

As the simplest nuclear environment that involves dynamics beyond the two-nucleon interactions, the ^{3}He nucleus provides a testing ground of our understanding of the three-nucleon force (3NF), sometimes highlighting flaws or omissions [1]. Significant theoretical effort has been made to accurately characterize three-nucleon systems, including two major methods that describe the process of electron scattering off A = 3 nuclei: plane wave impulse approximation (PWIA) [2–4] and exact non-relativistic Faddeev calculations [5–9]. The PWIA has typically shown good agreement with data at large four-momentum transfers. At low four-momentum transfers above the two-body ($p+d$) and three-body ($p+p+n$) breakup threshold, non-relativistic Faddeev calculations that fully include final-state interactions (FSI) and use realistic nucleon-nucleon potentials along with the meson-exchange currents (MEC), have been successful in describing the data.

Experimental measurements that can directly probe FSI, 3NF, and MEC would provide additional limits and further refinements to theoretical models. This can be done by identifying kinematic regions where effects due to these three mechanisms are expected to be large. Inclusive unpolarized cross section measurements made in the threshold region showed good agreement with theoretical predictions [10]. On the other hand, initial measurements of spin observables suggested missing elements in theoretical description, possibly due to MEC and FSI, which was improved in later, more precise measurements [11].

We report here a new precision measurement of the double-spin asymmetry of electron quasi-elastic scattering off the ^{3}He in the threshold region. It is the first such measurement in which the ^{3}He target was polarized longitudinally along the beam direction, probing a different combination of response functions than previously performed [11,12]. In such regions of low momentum transfer, rescattering between the nucleon that interacted with the virtual photon and the remaining nucleons can occur [5], providing a unique testing ground of FSI and MEC. In the following, we describe the formalism, experiment, data analysis, and the results.

For quasielastic scattering in which longitudinally polarized electrons scatter off a polarized ^{3}He target, the inclusive differential cross section can be expressed as [13]:

$$\frac{d\sigma}{d\Omega dE'} = \frac{\alpha^2\cos^2(\frac{\theta}{2})}{4E^2\sin^4(\frac{\theta}{2})}\{v_l R_L + v_t R_T - h\left[v_{T'}\cos\theta^* R_{T'} + 2v_{TL'}\sin\theta^*\cos\phi^* R_{TL'}\right]\}, \quad (1)$$

where α is the fine-structure constant, E is the initial electron energy, and θ is the electron scattering angle; R_T and R_L are the spin-averaged response functions, while $R_{T'}$ and $R_{TL'}$ are the spin-dependent response functions of the target; the terms v_i ($i = L, T, T', TL'$) are kinematic factors; and θ^* and ϕ^* are the polar and azimuthal angles of the nuclear target polarization vector in the laboratory frame, with $\hat{z}$ defined along the virtual-photon momentum $\hat{q}$ [14].

The spin-dependent asymmetry for a longitudinally polarized target is defined as

$$A = \frac{\sigma^{\uparrow\Uparrow} - \sigma^{\downarrow\Uparrow}}{\sigma^{\uparrow\Uparrow} + \sigma^{\downarrow\Uparrow}}, \quad (2)$$

where $\sigma^{\uparrow\Uparrow}$ and $\sigma^{\downarrow\Uparrow}$ are the cross section for scattering with the electron spin parallel and anti-parallel to the target spin, respectively. Substituting the expression for the cross section given in Eq. (1) into Eq. (2), the asymmetry can be written as:

$$A = -\frac{\cos\theta^* v_{T'} R_{T'} + 2\sin\theta^*\cos\phi^* v_{TL'} R_{TL'}}{v_L R_L + v_T R_T}. \quad (3)$$

The experiment reported here [14] was performed in Hall C of the Thomas Jefferson National Accelerator Facility (Jefferson Lab) in 2020. The original goal was to determine the first diffractive minima of both electric and magnetic form factors of ^{3}He by measuring the double spin asymmetry of e–^{3}He elastic scattering. Meanwhile, the experimental conditions provided an opportunity to also measure the double spin asymmetry of quasielastic scattering. A longitudinally polarized electron beam of 2.2 GeV energy was scattered off a 40-cm long longitudinally polarized ^{3}He target with approximately 12 amagats of density.

Scattered electrons were detected in the Super High Momentum Spectrometer (SHMS) at two scattering angles: 8.5° and 13°. The SHMS consists of five superconducting magnets [15] arranged in a DQQQD configuration. The first dipole (D) is a horizontal bender (HB) used to bend scattered electrons by a small angle (≈3 °) and allows the spectrometer to reach a minimum scattering angle of 5.5°. The remaining quadrupole (Q) elements are used for focusing of the scattered particles while the last dipole is used for momentum selection and deflects the particles into the SHMS detectors. The solid angle of the SHMS has a coverage of 4 msr along with a large momentum acceptance of $\Delta p/p = (-10, 22)\%$ [16].

The series of detectors in the SHMS provide tracking, timing, and particle identification of the scattered particles. The first detector is a pair of drift chambers that provide position and tracking information, which can be coupled with optics properties of the spectrometer to reconstruct the particles scattering angle, momentum, and the interaction position in the target. Following the drift chamber are two planes of hodoscopes, with each plane being comprised of vertical (Y) and horizontal (X) scintillator paddles and is used primarily as a trigger. A threshold gas Cerenkov detector and an electromagnetic calorimeter are used for particle identification. The combination of particle identification (PID) detectors can provide a clean discrimination of pions at 1000:1 while maintaining an electron detection efficiency of 99% [16]. Finally, the calorimeter energy resolution at these kinematic settings was shown to be around 5%, in line with the expected performance of $\approx 6\%/\sqrt{E}$, where E is the energy of the particle in GeV.

During the run period for this experiment, several measurements of the beam polarization were made in Hall C at a higher energy of 10.4 GeV. These measurements could be described by a fit to the beam polarization starting at the injector source and accounting for the polarization angle at the injector and the beam energy. This parameterization was consistent with additional beam-polarization measurements, with sub-percent uncertainties, that were performed in Hall A at an energy of 2.2 GeV. The beam polarization for this measurement was determined using the above fit evaluated at 1 pass in Hall C and yielded an average beam polarization of 88.2%. To estimate the associated

uncertainty, the previous experiments' systematic uncertainty was applied along with an additional 1% uncertainty, added in quadrature, accounting for possible shifts in beam energy, resulting in total fractional uncertainty, $\Delta P_b/P_b$, of 2.1% . The helicity of the polarized electron beam was delivered with a helicity-flip rate of 120 Hz during this experiment. Finally, an insertable half-wave plate was placed in the beamline which would produce a helicity of the electron beam that is opposite from when the half-wave plate is not inserted. The physics asymmetries between these two states should differ in their sign, thus providing a check for potential false asymmetries.

The target system included a gaseous polarized ^{3}He cell, along with an unpolarized reference cell, as well as additional solid targets used for calibration. The ^{3}He target was polarized via spin exchange optical pumping [17,18]. To ascertain the target polarization, a two-step process was used. First, the absolute polarization was determined through an Electron Paramagnetic Resonance (EPR) measurement, which served as a calibration point. Second, Adiabatic Fast Passage NMR measurements provide a relative polarization. NMR measurements can be taken more frequently during data collection, and when combined with the calibration constant from the EPR measurement, allows for a determination of the target polarization over time. The in-beam target polarization was found to vary between 35% and 50%, with an average of 46%. The systematic uncertainties were studied extensively and include contributions associated with the EPR/NMR calibration procedure, AFP losses, and the polarization evolution between the pumping chamber and target chamber during running. The total relative uncertainty of the target polarization was found to be $\Delta P_t/P_t < 4\%$.

Two tungsten collimators were placed adjacent to the target cell, on the SHMS side, in order to reduce background events that scattered off the unpolarized glass windows. In addition, a cut is applied on the reconstructed vertex position to further remove residual contributions from the entrance and exit windows of the target cell. After these selections, the contribution from window scattering was found to be negligible.

Data were collected at two primary kinematics, which provided asymmetries at four-momentum transfer squares $Q^2 = 0.1$ and $Q^2 = 0.2$ (GeV/c)^2. With the target spin oriented at 0°, the central θ^* for these settings were 76° and 77° respectively. In order to better balance the proportion of elastic and quasielastic events, selected scintillator paddles in the SHMS were turned off, reducing the acceptance of the spectrometer. The optimal paddle configuration was determined empirically by varying the enabled paddles and monitoring the ratio of elastic events to the total event yield.

Electrons were identified through PID cuts based on the gas Cerenkov and electromagnetic calorimeter detectors. A minimum response in the Cerenkov of 5 photoelectrons along with an E/p greater than 0.8, where E is the particle energy measured by the calorimeter and p is the reconstructed momentum, were required. Additionally, acceptance cuts were used to exclude regions not well constrained by the existing optics matrix and a reconstructed-vertex cut along the target length ($|z| \leq 15$ cm) was applied.

To form the asymmetry, yields were sorted based on the incident electron's helicity:

$$Y^+ = \frac{N^+}{Q^+ LT^+} \qquad Y^- = \frac{N^-}{Q^- LT^-}, \tag{4}$$

where N^+ (N^-) represents the number of detected electrons in + (-) beam helicity state, Q^+ (Q^-) and LT^+ (LT^-) the corresponding total incident beam charge and live time of the data acquisition system, respectively. The asymmetry can then be formed as:

$$A_{\text{raw}} = \frac{Y^+ - Y^-}{Y^+ + Y^-}. \tag{5}$$

To determine the event selection criteria on the acceptance and target variables, a single-spectrometer Monte Carlo (MC Single Arm) [19] was adapted to describe the experimental setup. To ensure a satisfactory description of the scintillator paddle configuration, the simulated events were compared with data in both the focal plane and the reconstructed target quantities. The individual contributions from simulated elastic and quasielastic scattering were combined and were consistent with data, providing confidence in our understanding of the experimental configuration.

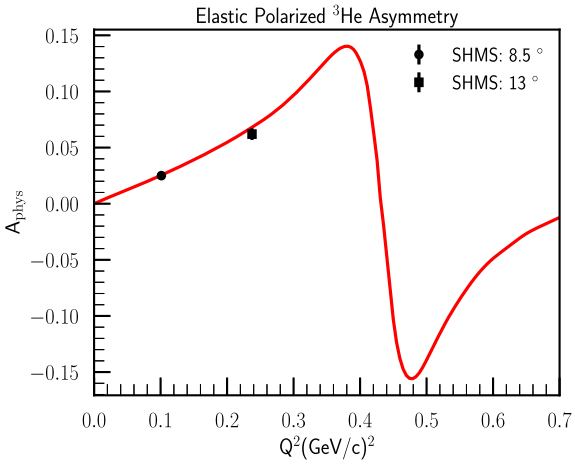

Fig. 1. Measured elastic asymmetry for the $Q^2 = 0.1$ and $Q^2 = 0.2$ (GeV/c)^2(red solid circle), along with a prediction for the asymmetry (red curve). The error bar includes both statistical and systematic uncertainties.

In order to separate the elastic from the quasielastic spectrum, the momentum distribution was combined with the two-dimensional information of the scattering angle vs. excitation energy where separation between the elastic and quasielastic peaks is evident.

The elastic asymmetry extracted from data provided an independent check of the product of the beam and the target polarizations, $P_b P_t$. Illustrated in Fig. 1 is the measured elastic asymmetry for the kinematic settings $Q^2 = 0.1$ and $Q^2 = 0.2$ (GeV/c)^2 along with a parameterization [20] for the elastic asymmetry utilizing form factors determined from a sum of Gaussians fits to world data [21]. There is an overall good agreement between the measured asymmetries and predictions at low Q^2, where the elastic form factors are well constrained, indicating that the product $P_b P_t$ is reasonably well understood. Due to the limited beam time, the Q^2 coverage was not high enough to cover the diffractive minima.

Combining the measured raw asymmetry with the beam and target polarizations, the quasielastic physics asymmetry was obtained as:

$$A_{\text{QE}} = \frac{A_{\text{raw}}}{P_b P_t}\left(\frac{1}{1-d_{\text{El}}}\right) - A_{\text{El}}\left(\frac{d_{\text{El}}}{1-d_{\text{El}}}\right), \tag{6}$$

where d_{El} and A_{El} are the fractional contribution from and the asymmetry of elastic scattering in the quasielastic event sample. The fractional contribution from elastic scattering events was determined through simulation by applying the same QE event selection criteria as the data. The extracted QE asymmetry was studied further as a function of the excitation energy of ^{3}He, defined as

$$E_x = \sqrt{M^2 + 2M\omega - Q^2} - M, \tag{7}$$

where M is the mass of ^{3}He and ω is the energy transfer. The two-body and three-body breakups correspond to excitation energies of 5.5 and 7.7 MeV, respectively. The results for the asymmetry are given in Tables 1 and 2, along with statistical and systematic uncertainties. The systematic uncertainties include contributions from elastic radiative tail subtraction, spectrometer acceptance, and beam and target polarizations ($P_b P_t$). The results are compared with three theoretical predictions in Fig. 2. In both figures, two arrows are included to indicate the location of the two- and three-body breakup respectively.

Of the three theoretical approaches considered, one is based on the relativistic plane-wave impulse approximation (PWIA) [2]. In this model, the nuclear structure is described using a spectral function derived from the AV18 nucleon–nucleon interaction [22], with Coulomb

Table 1
The measured QE asymmetry as a function of the excitation energy for $Q^2 = 0.1$ (GeV/c)^2.

E_x (MeV)	A	δA_{stat}	δA_{syst}
8.0	0.0182	0.0023	0.0013
13.0	0.0115	0.0015	0.0008
18.0	0.0072	0.0014	0.0005
23.0	0.0041	0.0013	0.0003
28.0	0.0038	0.0012	0.0003
33.0	0.0052	0.0011	0.0004
38.0	0.0033	0.0011	0.0002
43.0	0.0026	0.0011	0.0002
48.0	0.0029	0.0011	0.0002
53.0	0.0061	0.0012	0.0002

Table 2
The measured QE asymmetry as a function of the excitation energy for $Q^2 = 0.2$ (GeV/c)^2.

E_x (MeV)	A	δA_{stat}	δA_{syst}
8.0	0.0404	0.0042	0.0029
13.0	0.0266	0.0062	0.0019
18.0	0.0128	0.0057	0.0009
23.0	0.0090	0.0044	0.0006
28.0	0.0014	0.0039	0.0001
33.0	0.0057	0.0035	0.0004
38.0	0.0042	0.0031	0.0003
43.0	0.0086	0.0028	0.0006
48.0	0.0007	0.0025	0.0006
53.0	0.0038	0.0025	0.0006

effects included, and the electromagnetic form factors are taken from the Höhler parameterization [23]. However, PWIA is not expected to provide a reliable description of three-nucleon systems at low energies, where rescattering effects and FSI play an important role. The remaining two calculations [5,7] are based on nonrelativistic three-body scattering theory and explicitly include both FSI and MEC. These two approaches differ primarily in their choice of nuclear interaction: the calculations by Golak et al. [6] employ the AV18 interaction supplemented by the Urbana IX three-nucleon force, while those by Deltuva et al. [7,8] use the CD-Bonn interaction with explicit Δ-isobar excitation and include the proton–proton Coulomb force. Both calculations used electromagnetic form factors from Hammer et al. [24].

As can be seen in Fig. 2, both nonrelativistic Faddeev calculations have an overall good agreement with the data at both kinematics, while PWIA fails at lower excitation energies. This finding is consistent with a previous study at low Q^2, where the Faddeev calculations could explain the experimental data [11] considerably better than PWIA. A complete quantitative decomposition of the separate MEC, FSI, 3NF contributions is highly valuable. However, due to limitations in the calculation sets available for the present work, an independent isolation of each component was not available. A comparison of calculations performed with and without the Δ isobar and 3NF forces by [8] indicates that, for the present low-Q^2 threshold region and for this observable, those contributions are relatively small. This suggests that FSI and MEC are the dominant mechanisms. It is possible that there are differences in the magnitude of the underlying mechanisms (FSI, MEC, two- and three-body forces) between a longitudinally polarized target (reported here) and earlier measurements [11] where the target spin was polarized transverse to the $\vec{q}$ vector. Combining all available data sets may allow for a more detailed study of these individual mechanisms near the threshold region.

We report here a recent, precision measurement of the double-spin asymmetry in electron quasielastic scattering off a ^{3}He target. The measurement was done where the target was longitudinally along the beam direction, providing new data to which theoretical models can be compared against, thus testing the underlying scattering mechanisms in the threshold region. The asymmetries are presented as functions of the excitation energy and are compared with calculations using PWIA and Faddeev equations with two different nucleon-nucleon potential inputs. Both Faddeev-based calculations agree with the new data fairly well, though the PWIA agrees with data only at high excitation energies. We expect that the new data set, taken at relatively low energy and momentum transfer, will be confronted with incoming predictions based on two- and three-nucleon potentials as well as electromagnetic current operators derived consistently within chiral effective field theory.

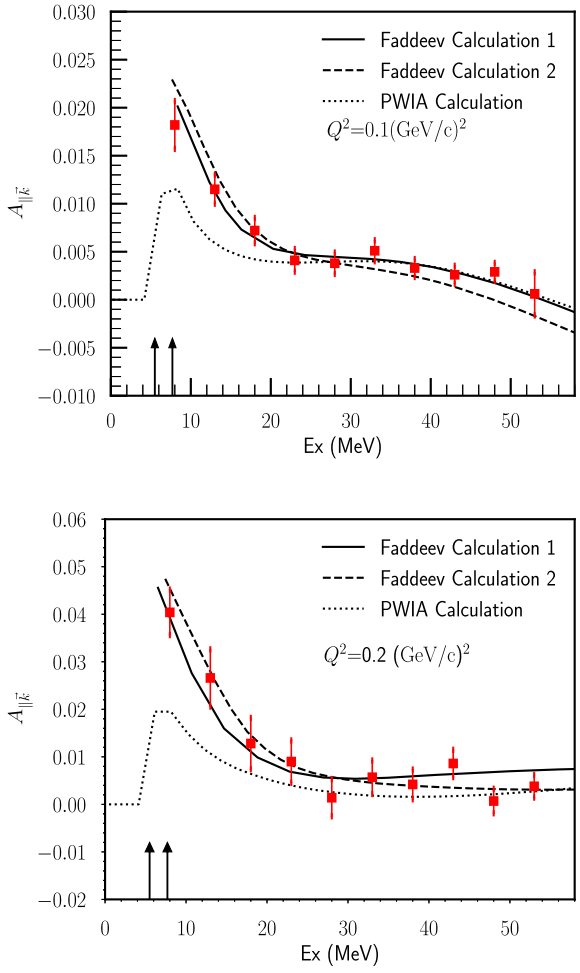

Fig. 2. Results on the quasielastic asymmetry, measured with the target spin aligned parallel to the beam direction, for $Q^2 = 0.1$ and $Q^2 = 0.2$ (GeV/c)^2, along with the theoretical predictions. The two arrows indicate the location of the two- and three-body breakup, respectively.

Declaration of competing interest

The authors declare that they have no known competing financial interests or personal relationships that could have appeared to influence the work reported in this paper.

Acknowledgments

We thank the Jefferson Lab Accelerator Division and Hall C technical staff for their support in successfully completing these measurements. This material is based upon work supported in part by the U.S. Department of Energy, Office of Science, Office of Nuclear Physics under contract numbers DE-AC05-06OR23177 (Jefferson Lab), DE-

FG02-99ER41101 (Univ. of Kentucky), and DE–SC0014434 (U. of Virginia). The work of J. Golak, R. Skibiński, and H. Witała (Kraków group) was supported by the National Science Centre, Poland, under Grant No. IMPRESS-U 2024/06/Y/ST2/00135, and by the Excellence Initiative - Research University Program at the Jagiellonian University in Kraków.

Data availability

Data will be made available on request.

References

[1] M. Mihovilovič, et al., Phys. Lett. B 788 (2019) 117–121. https://doi.org/10.1016/j.physletb.2018.10.063
[2] C. Ciofi degli Atti, E. Pace, G. Salmè, Phys. Rev. C 1 (1995). https://doi.org/10.1103/PhysRevC.51.1108
[3] A. Kievsky, E. Pace, G. Salmè, M. Viviani, Phys. Rev. C 56 (1997) 64–75. https://doi.org/10.1103/PhysRevC.56.64
[4] E. Pace, G. Salmè, S. Scopetta, A. Kievsky, Phys. Rev. C 64 (2001) 055203. https://doi.org/10.1103/PhysRevC.64.055203
[5] J. Golak, H. Wital, H. Kamada, D. Hüber, S. Ishikawa, W. Glöckle, Phys. Rev. C 52 (1995) 1216–1231. https://doi.org/10.1103/PhysRevC.52.1216
[6] J. Golak, R. Skibiński, H. Witała, W. Glöckle, A. Nogga, H. Kamada, Phys. Rep. 415 (2) (2005) 89–205. https://doi.org/10.1016/j.physrep.2005.04.005
[7] A. Deltuva, L.P. Yuan, J. Adam, P.U. Sauer, Phys. Rev. C 70 (2004) 034004. https://doi.org/10.1103/PhysRevC.70.034004
[8] A. Deltuva, Phys. Lett. B 835 (2022) 137552. https://doi.org/10.1016/j.physletb.2022.137552
[9] H. Witała, J. Golak, R. Skibiński, 2023, arXiv:2310.03433 [nucl-th]
[10] G.A. Retzlaff, et al., Phys. Rev. C 49 (1994) 1263–1271. https://doi.org/10.1103/PhysRevC.49.1263
[11] F. Xiong, et al., Phys. Rev. Lett. 87 (2001) 242501. https://doi.org/10.1103/PhysRevLett.87.242501
[12] W. Xu, et al., Phys. Rev. Lett. 85 (2000) 2900–2904. https://doi.org/10.1103/PhysRevLett.85.2900
[13] T.W. Donnelly, A.S. Raskin, Ann. Phys. (1986) 247–351.
[14] S.L. S. Barcus, D. Higinbotham, et al., Measurement of ^{3}He elastic electromagnetic form factor diffractive minima using polarization observables, 2020, https://doi.org/https://hallcweb.jlab.org/wiki/images/b/bc/PAC_Proposal_3He_Polarization_Observables.pdf.
[15] S. Wood, et al., Jefferson lab hall C standard equipment manual, 2019, https://doi.org/https://hallcweb.jlab.org/safety-docs/current/Standard-Equipment-Manual.pdf.
[16] S. Ali, et al., Nucl. Instrum. Methods Phys. Res. A 1083 (2026) 171070.
[17] T.G. Walker, W. Happer, Rev. Mod. Phys. 69 (2) (1997) 629–642. https://doi.org/10.1103/revmodphys.69.629
[18] J.T. Singh, P.A.M. Dolph, W.A. Tobias, T.D. Averett, A. Kelleher, K.E. Mooney, V.V. Nelyubin, Y. Wang, Y. Zheng, G.D. Cates, Phys. Rev. C 91 (2015) 055205. https://doi.org/10.1103/PhysRevC.91.055205
[19] Hall C SHMS single arm Monte Carlo, 2021, (https://github.com/JeffersonLab/mc_shms_single).
[20] S. Barcus, Ph.D. Thesis, College of William & Mary, 2019.
[21] A. Amroun, et al., Nucl. Phys. A 579 (3) (1994) 596–626. https://doi.org/10.1016/0375-9474(94)90925-3
[22] R.B. Wiringa, V.G.J. Stoks, R. Schiavilla, Phys. Rev. C 51 (1995) 38–51. https://doi.org/10.1103/PhysRevC.51.38
[23] G. Höhler, E. Pietarinen, I. Sabba-Stefanescu, F. Borkowski, G.G. Simon, V.H. Walther, R.D. Wendling, Nucl. Phys. B 114 (3) (1976) 505–534. https://doi.org/10.1016/0550-3213(76)90449-1
[24] H.-W. Hammer, U.-G. Meißner, Eur. Phys. J. A 20 (2004) 469–473. https://doi.org/10.1140/epja/i2003-10223-y